Simulation and design of a microphone array for beamforming on a moving acoustic source

Dick Petersen and Carl Howard

School of Mechanical Engineering, University of Adelaide, South Australia, Australia

ABSTRACT

A microphone array was designed and tested for the purpose of measuring the noise radiated by a moving acoustic source. Beamforming is used to enhance the signal-to-noise-ratio (SNR), with interfering sources moving at the same speed and along the same straight path as the measured source. A method is described for calculating moving source beampatterns that illustrates the SNR enhancement. The beamforming algorithm includes a de-Dopplerisation process to correct for the Doppler shift that occurs in the signals received at the array. This process leads to SNR enhancements that differ depending on whether the interfering source leads or lags the measured source when passing the array. The de-Dopplerisation process also causes grating lobes associated with spatial aliasing to move to lower frequencies when the interfering source leads the measured source. The described effects of the de-Dopplerisation process become more pronounced at higher speeds and when the interfering sources are farther away from the measured source. Hence, when designing a microphone array, it is important to conduct simulations that involve the use of a moving, rather than stationary, acoustic source, especially when the source moves at high speed. The modelling method presented in this paper was used to design an array which was tested in an anechoic chamber. The measured beampatterns for a stationary source are presented.

INTRODUCTION

Beamforming algorithms for moving acoustic sources, such as aircraft (Howell et al., 1986; Guérin et al., 2006; Guérin & Siller, 2008; Fleury & Bulté, 2011; Siller, 2012) and trains (Brühl & Röder, 2000), have been successfully developed. These algorithms include a de-Dopplerisation process that corrects for the Doppler shift in the received acoustic signals. Most of the research into moving source beamforming has considered the localisation of sources, and has used source-array arrangements that result in gradually changing Doppler shifts at the array microphones.

The beamforming method considered in this paper is a source enhancement rather than localisation technique (Johnson & Dudgeon, 1993, page 3). The microphone array is located close to the path along which the source travels, which results in Doppler shifts at the array microphones that change more rapidly in comparison to previous work (Howell et al., 1986; Brühl & Röder, 2000; ; Guérin et al., 2006; Guérin & Siller, 2008; Fleury & Bulté, 2011; Siller, 2012). Guérin & Weckmüller (2008) have noted that de-Dopplerisation process causes the side-lobes in the point-spread function to smear into lower and higher frequencies, depending on whether the interfering source leads or lags the measured source. The effect of this side-lobe smearing on the beamforming results has not been analysed in detail in previous research, perhaps because it was not significant for the considered source-array arrangements. This paper shows that it can have a significant effect for source-array arrangements that result in rapidly changing Doppler shifts at the array microphones.

A methodology for simulating and analysing the performance of a microphone array used for measuring the noise radiated by a moving acoustic source is presented. A moving source beamforming algorithm is used to enhance the signal-to-noise-ratio (SNR) beyond that of a single microphone output, with interfering sources moving at the same speed and along the same path as the measured source on which the array's beam is steered. The design methodology was used to design and build a microphone array, which was subsequently tested in an anechoic chamber. Measured beampatterns are presented for a stationary acoustic source.

SIMULATION OF ARRAY PERFORMANCE

Source and array arrangement

Figure 1 illustrates the arrangement of the acoustic sources and the microphone array assumed in the modelling.

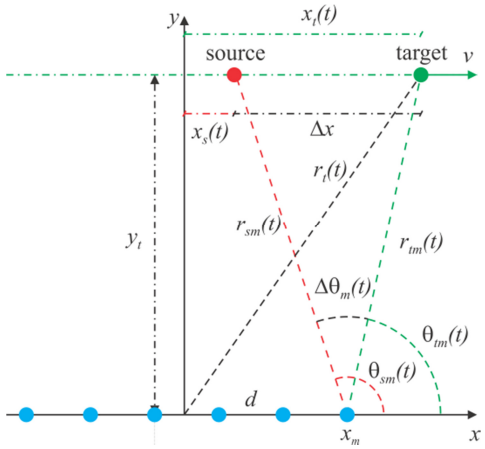

Figure 1 – Source and array arrangement assumed in modelling: (*red dot*) Source moving at a speed v m/s along straight line parallel to array at distance y_t; (*green dot*) Moving target location on which the beam of the array is steered; (*blue dots*) linear array consisting of M microphones spaced d metres apart.

In the modelling, a linear array consisting of M microphones equispaced at d metres is considered. The source moves at a constant speed v m/s in the positive x direction along a straight line parallel to the array at a distance y_t. The required length of view of the measured source is $L = 2x_L$ and extends from $-x_L$ to x_L. The path of the measured source is known a-priori and defines the moving target loca-

tion $[x_t(t), y_t]$ on which the array's beam is steered. The source is located at $[x_s(t), y_t]$ with $\Delta x = x_s(t) - x_t(t)$ the source-to-target distance. Using these definitions, the location of the measured source corresponds to a source-to-target distance $\Delta x = 0$. Interfering sources that lead or lag the measured source correspond to source-to-target distances $\Delta x > 0$ or $\Delta x < 0$, respectively.

Simulation of received signals

This section describes the simulation of the acoustic source signals received at the microphones at equispaced times $t = nT_s$, with T_s the sample time (Howell et al., 1986). Suppose a source is at position $x_s(0)$ at $t = 0$. The propagation time for a source signal $s(\tilde{t}_m)$ emitted from position $x_s(\tilde{t}_m) = x_s(0) + v\tilde{t}_m$ at time $\tilde{t}_m$ to a microphone located at x_m is

$$t - \tilde{t}_m = \frac{\sqrt{(x_s(0) + v\tilde{t}_m - x_m)^2 + y_t^2}}{c} = \frac{r_{sm}(\tilde{t}_m)}{c} \quad (1)$$

with $r_{sm}(\tilde{t}_m)$ the distance between the source and microphone m at time $\tilde{t}_m$ as shown in Figure 1, c the speed of sound, and t the time at which the signal is received at microphone m. Substituting $x_s(0) = x_s(t) - vt + x_m$ into Equation (1), this becomes

$$t - \tilde{t}_m = \frac{\sqrt{\left(x_s(t) - v(t - \tilde{t}_m)\right)^2 + y_t^2}}{c} \quad (2)$$

By squaring Equation (2) and solving for the propagation time $t - \tilde{t}_m$, it can be shown that

$$\tilde{t}_m = t + \frac{x_s(t)v - \sqrt{c^2 x_s(t)^2 + (c^2 - v^2)y_t^2}}{c^2 - v^2} \quad (3)$$

Equation (3) can be used to calculate the non-equispaced emission times $\tilde{t}_m$ and locations $x_s(\tilde{t}_m)$ corresponding to a set of equispaced reception times t, for each microphone. Given the emission times $\tilde{t}_m$, the moving source signal received at microphone m at equispaced times t is calculated as

$$p_m(t) = \frac{s(\tilde{t}_m)}{4\pi r_{sm}(\tilde{t}_m)} \quad (4)$$

where a point source and spherical spreading have been assumed. When simulating the received microphone signals as defined by Equations (1) to (4), the Doppler shift caused by movement of the source is included in the signals.

In Equation (4), the source signal can be evaluated exactly at the non-equispaced times $\tilde{t}_m$ when it is modelled as a deterministic signal but not when it is modelled as a random signal. For this case, the source signal $s(\tilde{t}_m)$ is simulated by generating a random source signal $s(t)$ and interpolating it at the non-equispaced times $\tilde{t}_m$. Piecewise cubic spline interpolation and a sufficiently high sampling frequency are used to obtain good results over the frequency range of interest.

De-Dopplerising of received signals

In the beamforming algorithm, the microphone signals are de-Dopplerised to correct for the Doppler shift associated with the measured source at the moving target location $x_t(t)$. With the measured source at position $x_t(0)$ at time $t = 0$, signals emitted at equispaced times $t = nT_s$ arrive at microphone m at non-equispaced times

$$\tau_{tm} = t + \frac{\sqrt{(x_t(0) + vt - x_m)^2 + y_t^2}}{c} = t + \frac{r_{tm}(t)}{c} \quad (5)$$

with $r_{tm}(t)$ the distance between the target location and microphone m at time t, as shown in Figure 1. The signal received at microphone m at equispaced times $t = nT_s$ is now de-Dopplerised by interpolating the signal at the non-equispaced times τ_{tm} defined in Equation (5). The resulting de-Dopplerised signal is denoted by $p_{d,m}(t)$. Piecewise cubic spline interpolation is used in the de-Dopplerisation process.

Frequency content of de-Dopplerised signals

A signal of frequency f_0 emitted by a source from location $x_s(\tilde{t}_m)$ is received at microphone m at an apparent frequency

$$f_{a,m}(t) = \frac{c}{c + v\cos\theta_{sm}(\tilde{t}_m)} f_0 \quad (6)$$

with $\theta_{sm}(\tilde{t}_m)$ the angle between the source path and the line of sight from the microphone to the source, as illustrated in Figure 1. When de-Dopplerising the received signal for the measured source at the moving target location $x_t(t)$, the De-dopplerised signal has an instantaneous frequency given by

$$f_{d,m}(t) = \frac{c + v\cos\theta_{tm}(\tilde{t}_m)}{c + v\cos\theta_{sm}(\tilde{t}_m)} f_0 \quad (7)$$

with $\theta_{tm}(\tilde{t}_m)$ the angle between the source path and the line of sight from the microphone to the target location, as shown in Figure 1. Equation (7) shows that the de-Dopplerisation process is not effective for an interfering source since the angle $\theta_{sm} \neq \theta_{tm}$ in this instance, or equivalently, the source-to-target distance $\Delta x \neq 0$ in Figure 1. It also shows that for an interfering source, the instantaneous frequency of the de-Dopplerised signal is always higher than the emitted frequency f_0 when it lags the measured source ($\Delta x < 0$), and lower when it leads ($\Delta x > 0$). The bandwidth of the de-Dopplerised signal is also proportional to both the source speed v and source-to-target distance Δx.

Moving source beampattern

The de-Dopplerisation process effectively time-aligns the microphone signal components due to the measured source to the common moving target location. This is effectively the same as the delay part of the commonly used delay-and-sum beamforming method (Johnson & Dudgeon, 1993, page 112). The final beamformed output $p_b(t)$ is now calculated by summing the de-Dopplerised microphone signals as

$$p_b(t) = \frac{1}{M}\sum_{m=1}^{M} p_{d,m}(t) \quad (8)$$

By simulating the beamformed output $p_b(t)$ for various source-to-target distances Δx and calculating its power spectral density, a moving source beampattern is generated that enables comparison of the beamformed signal levels for measured ($\Delta x = 0$m) and interfering ($\Delta x \neq 0$m) sources of the same source strength. Normalising the beampattern to the beamformed output for the measured source ($\Delta x = 0$m) illustrates the SNR enhancement that is achieved for an interfering source at a distance Δx from the measured source.

Quasi-stationary source beampattern

For the case of a stationary source, it is convenient to write the received source signal at microphone m in complex polar notation as (Johnson & Dudgeon, 1993, page 17)

$$P_m(f_0) = \frac{Ae^{i2\pi f_0 r_{sm}/c}}{4\pi r_{sm}} \quad (9)$$

with A the amplitude of the complex source signal s. For a source at the target location, the time delay Δ_m between the source signal received at microphone m and the array centre is given by

$$\Delta_m = \frac{r_{tm} - r_t}{c} \tag{10}$$

with r_t the distance between the target and centre of the array as shown in Figure 1. The delay-and-sum beamformed output for the stationary source case is now calculated directly in the frequency domain as (Johnson & Dudgeon, 1993, page 133)

$$P_b(f_0) = \frac{1}{M}\sum_{m=1}^{M} P_m(f_0) e^{-i2\pi f_0 \Delta_m} \tag{11}$$

A spatial average beamformed output $\bar{P}_b(f_0)$ is calculated by averaging the beamformed output for N target locations $[x_{ti}, y_t]$, such that

$$\bar{P}_b(f_0) = \frac{1}{N}\sqrt{\sum_{i=1}^{N} P_{bi}(f_0)^2} \tag{12}$$

with $P_{bi}(f_0)$ the beamformed output for target location x_{ti} calculated using Equations (9) to (11). The N target locations are equispaced over the length of view. By simulating the spatial average beamformed output $\bar{P}_b(f_0)$ for various source-to-target distances Δx and emitted frequencies f_0, a quasi-stationary source beampattern is generated.

EXAMPLE SIMULATIONS

This section presents example results to illustrate the described array simulation method. The maximum and minimum frequencies of interest are $f_{\max}$ and $f_{\min} = 0.5f_{\max}$, respectively. The array consists of $M = 6$ microphones spaced at $d = 0.5\lambda_{\min}$ with $\lambda_{\min} = c/f_{\max}$ the minimum wavelength of interest. The sources move at speeds ranging from $v = 0.016c$ to $0.13c$ at a distance $y_t = 28\lambda_{\min}$ from the array, which results in a rapidly changing Doppler shift. The required length of view of the measured source is $L = 122\lambda_{\min}$. The source signals received at the microphones are simulated using a sample frequency $F_s = 8.2f_{\max}$.

Moving and quasi-stationary source beampatterns

Moving source beampatterns were calculated for the minimum and maximum speeds of $v = 0.016c$ and $0.13c$, respectively. The acoustic source signal $s(t)$ was modelled as a white-noise sequence with unit standard deviation and results were averaged over 20 sequences. The resulting moving source beampatterns are illustrated in Figure 2. The quasi-stationary source beampattern, which was calculated from Equation (12) using $N = 27$ target locations, is included for comparison. The beampatterns have been normalised to the beamformed output for the measured source ($\Delta x = 0$m) to illustrate the SNR enhancement that is achieved for interfering sources at a distance Δx from the measured source.

The quasi-stationary source beampattern in Figure 2(c) is symmetrical about $\Delta x = 0$m. This symmetry is not observed in the moving source beampatterns in Figure 2(a) and (b). Comparing these beampatterns shows that the asymmetry is more pronounced at the higher speed and at larger source-to-target distances. In other words, for interfering sources at the same absolute distance $|\Delta x|$ to the measured source, the SNR enhancement is worse when the interfering source lags rather than leads the measured source, with the difference increasing at higher speeds and larger distances Δx.

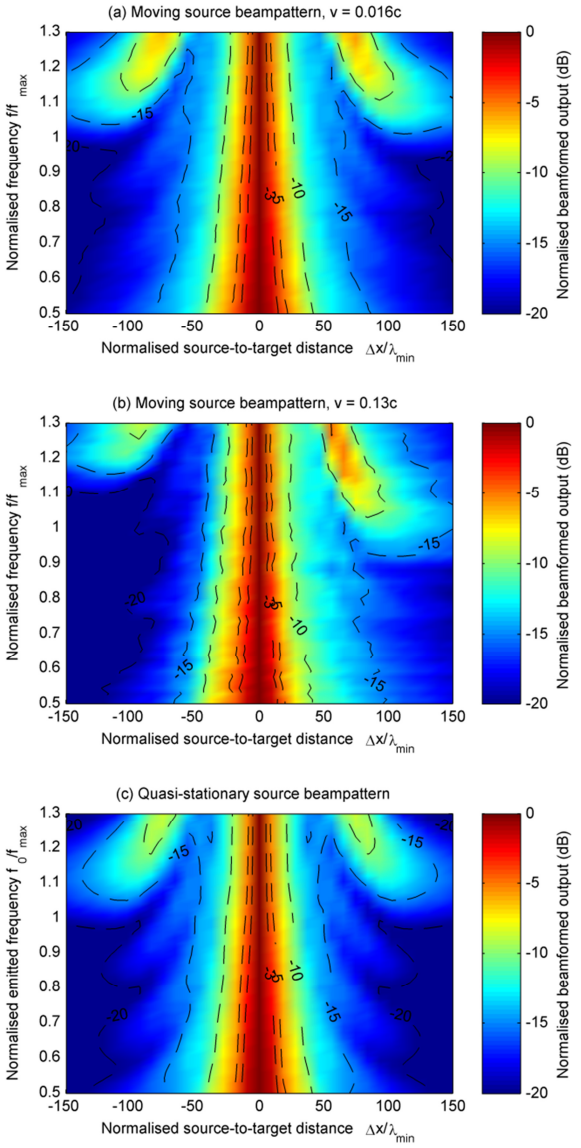

Figure 2 – Moving and quasi-stationary source beampatterns. The source moves at a speed $v = 0.016c$ or $0.13c$ at a distance $y_t = 28\lambda_{\min}$ from the array. The array consists of $M = 6$ microphones spaced at $d = 0.5\lambda_{\min}$. The length of view is $L = 122\lambda_{\min}$.

The difference between the SNR enhancement achieved for leading and lagging interfering sources is more clearly visualised in Figure 3. This figure compares the SNRs enhancement for the leading and lagging interfering source cases by evaluating the beampatterns in Figure 2 at a frequency $0.7f_{\max}$ and plotting the results against absolute source-to-target distance $|\Delta x|$. The results in Figure 3 show that the SNR enhancement is better when the interfering source lags ($\Delta x < 0$) rather than leads ($\Delta x > 0$) the measured source at $\Delta x = 0$, with the difference becoming more noticeable at higher speeds v and larger source-to-target distances $|\Delta x|$. To give an example, Figure 3 shows that for a source speed $v = 0.13c$ and source-to-target distance $|\Delta x = 100\lambda_{\min}|$, the SNR enhancement is 20 dB when the interfering source lags the measured source and 17 dB when it leads.

The moving and quasi-stationary source beampatterns in Figure 2 all have grating lobes associated with spatial aliasing. Figure 2(a) and (b) show that the grating lobes in the

moving source beampattern shift towards higher frequencies when the interfering source lags the measured source ($\Delta x < 0$) and lower frequencies when it leads ($\Delta x > 0$), with the frequency shift increasing at higher source speeds.

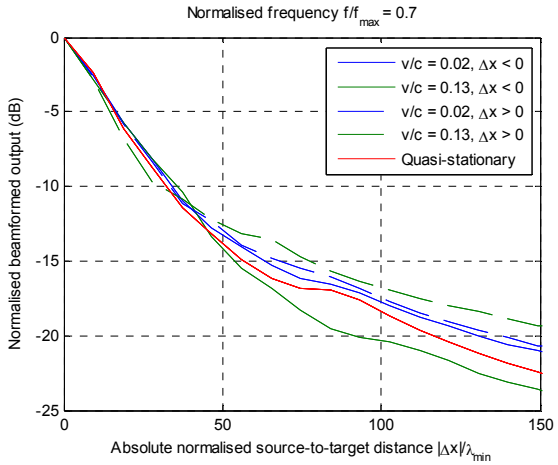

Figure 3 – Moving and quasi-stationary source beampatterns evaluated at a frequency $0.7f_{\max}$. The source moves at a speed $v = 0.016c$ or $0.13c$ at a distance $y_t = 28\lambda_{\min}$ from the array. The array consists of $M = 6$ microphones spaced at $d = 0.5\lambda_{\min}$. The length of view is $L = 122\lambda_{\min}$.

Figure 2(a) shows that at the low speed, the grating lobe does not significantly move into the frequency range of interest below $f_{\max}$. This indicates that the $0.5\lambda_{\min}$ microphone spacing is sufficient for preventing spatial aliasing problems at the low speed. At the higher speed, the grating lobe in Figure 2(b) does start moving into the frequency range of interest for interfering sources that lead the measured source ($\Delta x > 0$). As an example of its effect, the SNR enhancement for an interfering source at $\Delta x = 100\lambda_{\min}$ reduces from 17 dB to 12 dB at a frequency $f_{\max}$, as the source speed increases from $v = 0.016c$ to $0.13c$. In the quasi-stationary source beampattern, the SNR is 19 dB for this case.

De-Dopplerisation of received signals

The features of the moving source beampattern discussed in the previous section will now be explained by analysing the de-Dopplerisation of the measured and interfering source signals received at the array. To this end, results for a sinusoidal source signal $s(t)$ of unit amplitude and frequency $f_0 =$ cy $f_0 = 0.7f_{\max}$ are presented.

Figure 4 illustrates the location $x_s(\tilde{t}_m)$ of the measured source at the non-equispaced emission times $\tilde{t}_m$ corresponding to the equispaced received times t, which were defined in Equation (3), for speeds $v = 0.02c$ and $0.13c$. The apparent frequency of the measured source signal received at the array is also shown. The red line indicates the emitted frequency. The time has been normalised against the time it takes for the measured source to travel along the length of view, i.e. L/v.

The results in Figure 4 show that at the lower speed, the non-equispaced source emission locations $x_s(\tilde{t}_m)$ are almost evenly distributed over the length of view. Consequently, the corresponding Doppler shift is negative and positive for nearly the same amount of time at low speeds. For the higher speed $v = 0.13c$, the non-equispaced source locations are more unevenly distributed over the length of view, i.e. there are more locations at which the measured source is receding from the array. This means that the Doppler shift is negative for a longer proportion of time at the higher speed. The increasingly uneven distribution of the measured source emission locations over the length of view as speed increases causes the non-symmetries in the moving source beampattern in Figure 2 to become more pronounced at higher speeds.

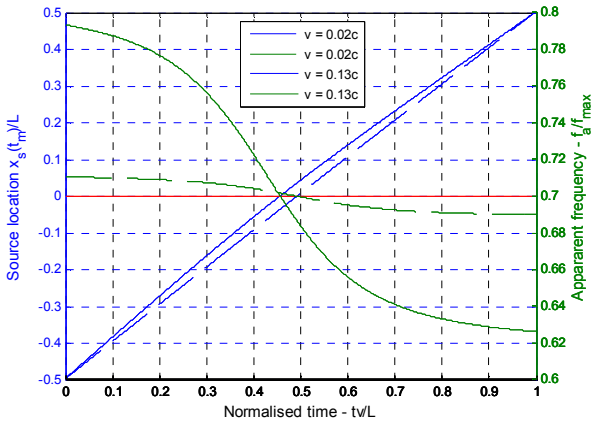

Figure 4 – (*Blue*) Location $x_s(\tilde{t}_m)$ of the measured source at the non-equispaced emission times $\tilde{t}_m$ corresponding to the equispaced times t. (*Green*) Apparent frequency of the measured source signals received at the array microphones. (*Red*) Emitted frequency $0.7f_{\max}$

Figure 5(a) and (b) illustrate the instantaneous frequency (Cohen 1995) and sound pressure level of the received and de-Dopplerised signals for the measured and interfering sources, at the higher speed $v = 0.13c$. Figure 5(c) shows the absolute Doppler shift that remains in the interfering source signals after de-Dopplerising for the measured source at the target location. Interfering sources at absolute source-to-target distances $|\Delta x| = 25\lambda_{\min}$ and $150\lambda_{\min}$ are considered to enable comparison of the leading and lagging source cases for both small and large source-to-target distances.

Figure 5(a) shows that the apparent frequency of the received signal from the measured source changes from $0.79f_{\max}$ to $0.63f_{\max}$ as the source approaches and recedes from the array at a speed $v = 0.13c$. After de-Dopplerisation, the frequency of the measured source signal equals the emitted frequency $0.7f_{\max}$ over the entire length of view as illustrated in Figure 5(b).

Figure 5(a) illustrates that for an interfering source that leads the measured source ($\Delta x < 0$) as they pass the array, the Doppler shift is always larger in comparison to the Doppler shift for the measured source at the target location, which is corrected for in the de-Dopplerisation process. For an interfering source that leads the measured source ($\Delta x < 0$), it is always smaller. As a result, the de-Dopplerised signals for the interfering sources shown in Figure 5(b) have a time-varying instantaneous frequency which differs from the emitted frequency. The instantaneous frequency is always higher than the emitted frequency $0.7f_{\max}$ when the interfering source lags the measured source ($\Delta x < 0$), and lower when it leads. Note that these observations follow directly from Equation (7).

Figure 5(c) illustrates that the Doppler shift that remains in the signals after the de-Dopplerisation process is generally greater for an interfering source that lags rather than leads the measured source. It also shows that this difference is more noticeable as the distance between the measured and interfering sources increases.

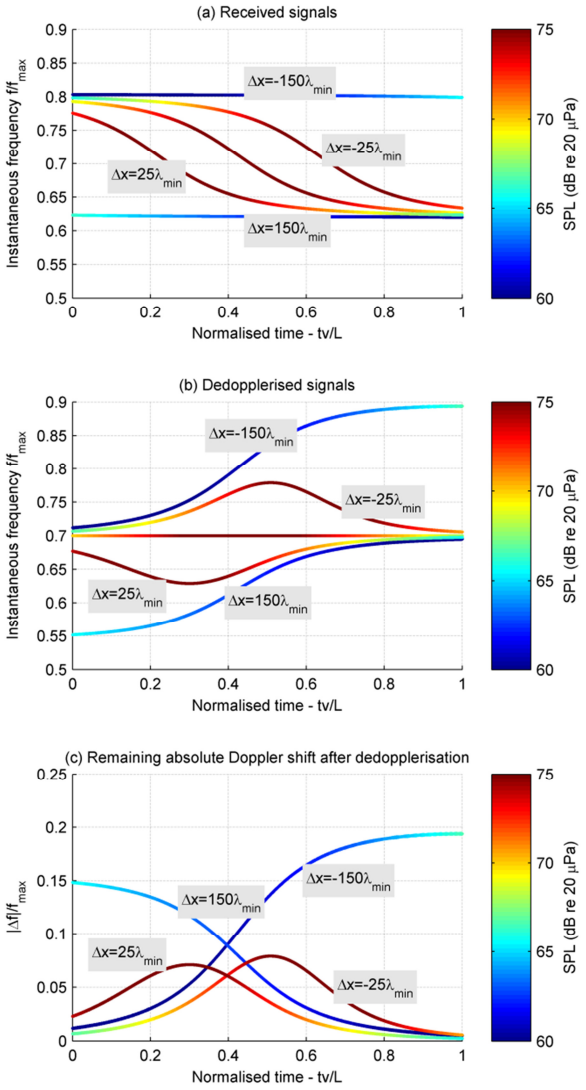

Figure 5 – (a) Apparent frequency of target and noise source signals received at microphone 3 for a source speed $v = 0.13c$. (b) Frequency of measured and interfering source signals after de-Dopplerisation for the measured source at $\Delta x = 0$m. (c) Remaining absolute Doppler shift after de-Dopplerisation for the measured source.

Figure 6 presents the sound pressure level (SPL) spectra of the received, de-Dopplerised and beamformed signals for a range of source-to-target distances Δx, for one of the array microphones and the higher speed $v = 0.13c$. The dashed white line indicates the emitted frequency $0.7f_{\max}$ and the dash-dotted white lines the source-to-target distances for which results were presented in Figure 5. The spectral distributions in Figure 6(a) and (b) concur with the instantaneous frequency and amplitude plots presented in Figure 5.

In Figure 6(b), a narrowband peak is visible at $\Delta x = 0$m and the emitted frequency $0.7f_{\max}$ indicating the de-Dopplerisation has been successful for the measured source. The de-Dopplerisation process is not effective for interfering sources at $\Delta x \neq 0$m with the de-Dopplerised signal spectra becoming increasingly broadband as the distance between the measured and interfering sources increases. Furthermore, the de-Dopplerised signals have energy only above the emitted frequency for a lagging interfering source ($\Delta x < 0$) and only below the emitted frequency for a leading interfering source ($\Delta x < 0$). Since the beamformed signal is calculated by averaging the de-Dopplerised signals, this also applies to the beamformed signal spectra in Figure 6(c). The spreading of interfering source energy into frequencies that are higher and lower than the emitted frequency explains the asymmetries in the moving source beampattern shown in Figure 2(b).

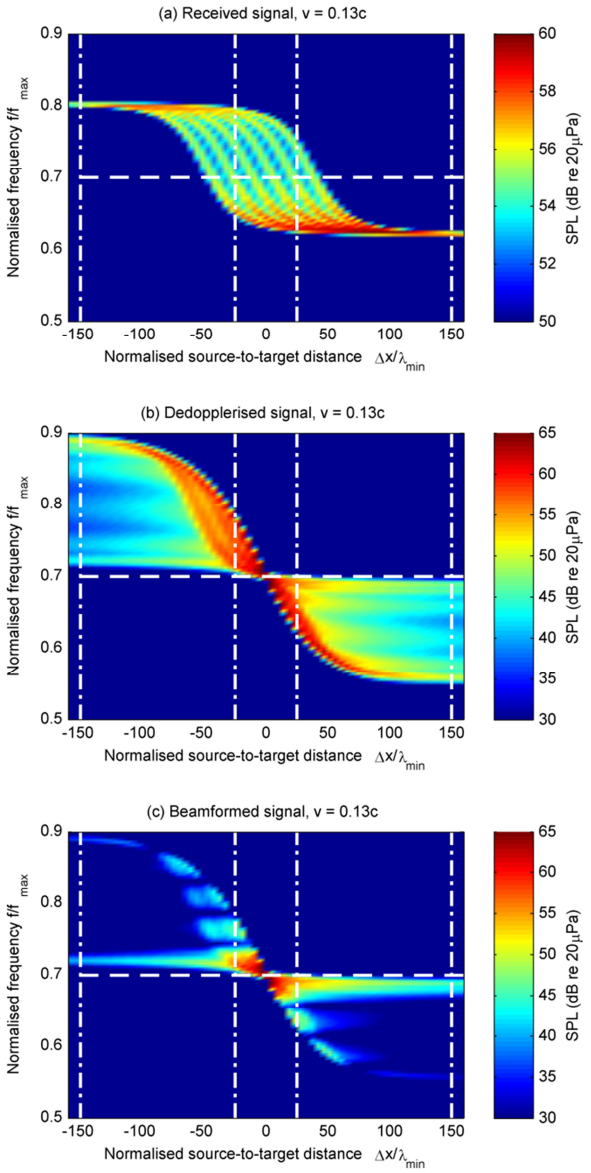

Figure 6 – SPL spectra of the received (a), De-dopplerised (b) and beamformed (c) source signals for a source speed $v = 0.13c$. The source emits a sinusoid at frequency $f_0 = 0.7f_{\max}$ and moves at a distance $y_t = 28\lambda_{\min}$ from the array and Δx from the target location. The array consists of $M = 6$ microphones spaced at $d = 0.5\lambda_{\min}$.

De-dopplerised signal components that add coherently in the beamformed output give rise to spectral components in Figure 6(b) and (c) that are of the same level. Comparing these spectra shows that the de-Dopplerised signal components add coherently near the emitted frequency $0.7f_{\max}$ and increasingly incoherently away from the emitted frequency.

For the same absolute source-to-target distance, Figure 6(b) shows that a leading interfering source ($\Delta x < 0$) has more energy near the emitted frequency, where the de-Dopplerised signals add coherently, than a lagging interfering source ($\Delta x < 0$). As a result, the SNR enhancement achieved on a leading interfering source is smaller than on a lagging interfering source at the same absolute source-to-target distance. The difference is more pronounced for interfering sources

that are farther away from the measured source. Going back Figure 5(c), this effect occurs because the Doppler shift that remains after de-Dopplerisation is generally smaller for an interfering source that leads rather than lags the measured source, with the difference increasing at larger source-to-target distances.

For completeness, Figure 7 presents the sound pressure level (SPL) spectra of the de-Dopplerised signals for the lower speed $v = 0.016c$, for one of the array microphones. Compared to the higher speed result illustrated in Figure 6(b), the spectral distributions for interfering sources at the same absolute source-to-target distance is more symmetrical about the emitted frequency. Furthermore, the spreading of interfering source energy into higher and lower than emitted frequencies is much smaller, due to the lower speed. This results in a moving source beampattern in Figure 2 that is more symmetrical for the lower speed compared to the higher speed.

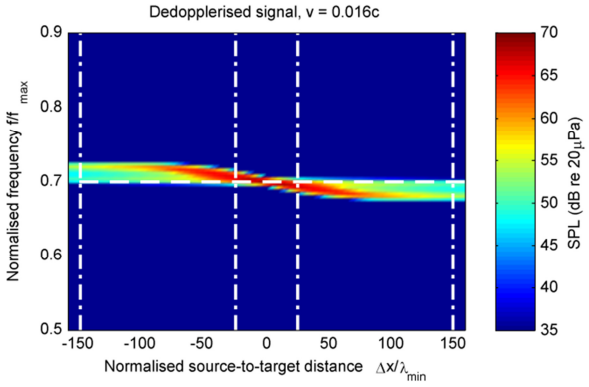

Figure 7 – SPL spectra of the De-dopplerised source signals for a source speed $v = 0.016c$. The source emits a sinusoid at frequency $f_0 = 0.7f_{\max}$ and moves at a distance $y_t = 28\lambda_{\min}$ from the array. The array consists of $M = 6$ microphones spaced at $d = 0.5\lambda_{\min}$.

Reducing effect of grating lobes

Figure 2(b) illustrates that at the higher speed $v = 0.13c$, the grating lobe on the leading interfering source side ($\Delta x > 0$) has shifted into the frequency range of interest in the moving source beampattern. This is caused by the de-Dopplerisation process which moves source energy into frequencies that are lower than the emitted frequency for an interfering source that leads the measured source, as illustrated in Figure 6(b) and (c). An array that is used for high speed applications thus needs smaller microphone spacing than the $0.5\lambda_{\min}$ criterion normally used for stationary source arrays if the grating lobe should not shift into the frequency range of interest.

Figure 8 presents the moving source beampattern at the higher speed $v = 0.13c$ with the microphone spacing reduced to $0.5\lambda^r_{\min}$ with $\lambda^r_{\min} = (c - v)/f_{\max}$ the minimum apparent wavelength of the source signals received at the array. In other words, the microphone spacing is reduced to prevent spatial aliasing at the highest apparent frequency that occurs in the received source signals for a maximum emitted frequency of interest $f_{\max}$. The results illustrate that reducing the microphone spacing effectively prevents the grating lobe on the leading interfering source side ($\Delta x > 0$) from shifting into the frequency range of interest in the moving source beampattern.

Number of microphones

Figure 9 illustrates the change in the moving and quasi-stationary source beamformed outputs as the number of array microphones M increases. Results at the minimum frequency of interest $f_{\min}$ are shown because the main lobe is widest at this frequency of interest. The source moves at the highest speed $v = 0.13c$ at a distance $y_t = 28\lambda_{\min}$ from the array and emits a white-noise sequence. The microphones are spaced at $d = 0.5\lambda_{\min}$.

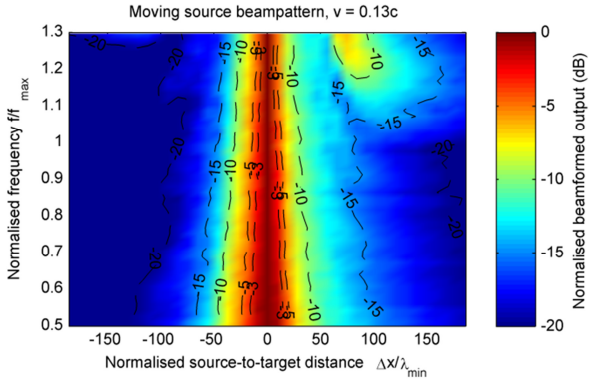

Figure 8 – Moving source beampattern with microphone spacing reduced from $0.5c/f_{max}$ to $0.5(c - v)/f_{\max}$. The source emits a white-noise sequence and moves at a speed $v = 0.13c$ at a distance $y_t = 28\lambda_{\min}$ from the array which consists of $M = 6$ microphones.

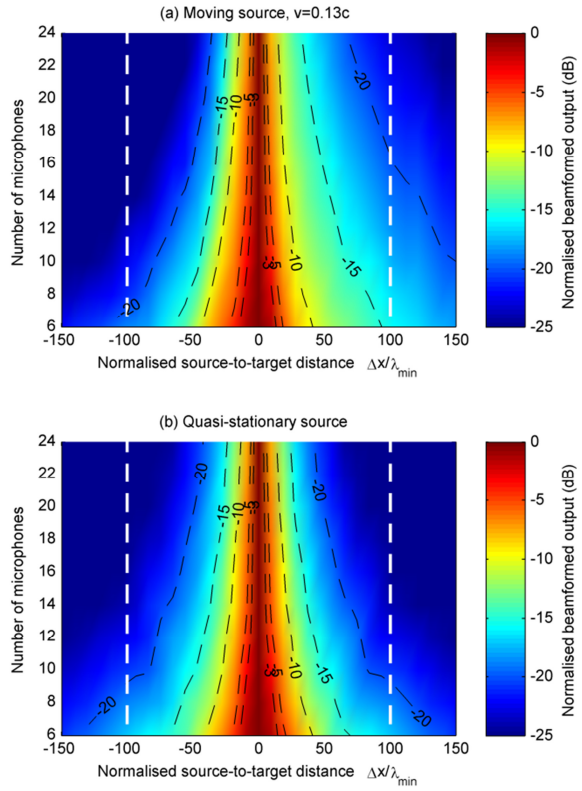

Figure 9 – Moving and quasi-stationary source beamformed outputs for increasing number of microphones M at the minimum frequency of interest $f_{\min}$. The source emits a white-noise sequence and moves at a speed $v = 0.13c$ at a distance $y_t = 28\lambda_{\min}$ from the array. The microphones are spaced at $d = 0.5\lambda_{\min}$.

As an example, assume the design aim is to achieve a SNR enhancement of at least 20 dB for an interfering source moving at an absolute distance $|\Delta x| = 100\lambda_{\min}$ from the measured source. The considered source-to-target distances are indicated by the white dashed lines in Figure 9. Based on the quasi-stationary target results in Figure 9(b), $M = 9$ microphones are required to achieve the design aim. However, the moving source result in Figure 9(a) shows that the number of microphones may be lowered to $M = 7$ when the interfering

source lags the measured source and, more significantly, needs to be increased to $M = 16$ when it leads. This example illustrates the importance of conducting moving source beampattern modelling when designing an array, especially for high speed applications.

Practical limit on microphone spacing

In the practical design of the array, the microphone spacing was unfortunately limited to $d = 0.58\lambda_{\min}$. Figure 10 shows the moving source beampatterns for this microphone spacing while using either $M = 6$ or 30 microphones. The source moves at the higher speed of $v = 0.13c$.

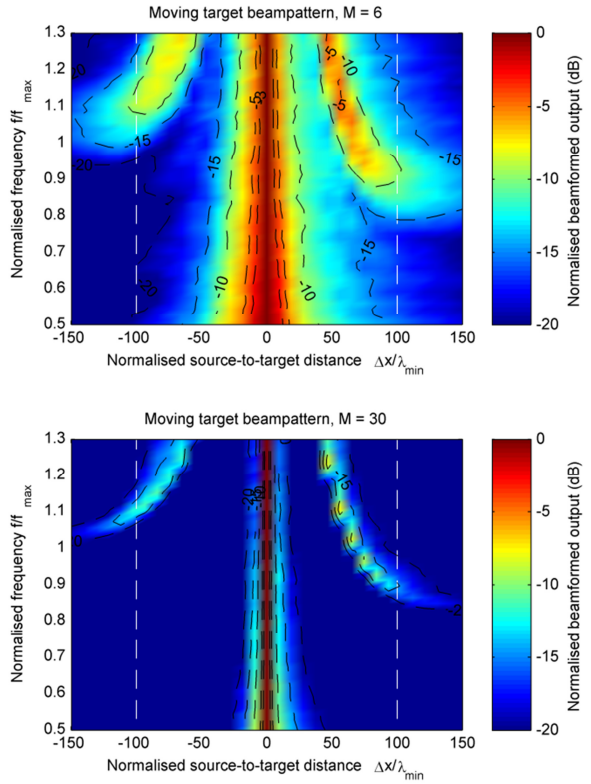

Figure 10 – Moving source beampatterns with either $M = 6$ or 30 array microphones spaced at $d = 0.58\lambda_{\min}$. The source emits a white-noise sequence and moves at a speed $v = 0.13c$ at a distance $y_t = 28\lambda_{\min}$ from the array.

Figure 10(a) shows that increasing the microphone spacing to $0.58\lambda_{\min}$ results in grating lobes that, in comparison to the result shown in Figure 2(b) for a spacing of $0.5\lambda_{\min}$, have moved further into the frequency range of interest below $f_{\max}$. As the microphone spacing could not be reduced and the distance y_t could not be increased, the only way to reduce the effect of the grating lobe was to use more microphones as illustrated in Figure 10(b). This narrows the main beam width thereby improving the spatial resolution.

Revisiting the design example from the previous section, the SNR enhancement achieved on an interfering source at $\Delta x = 100\lambda_{\min}$ increases from about 10 to 15dB when using 6 instead of 30 microphones. More microphones are needed to achieve the 20dB design aim.

EXPERIMENTAL TESTING

Experimental set-up

A microphone array consisting of $M = 30$ microphones (BSWA MP401) spaced at $d = 0.58\lambda_{\min}$ was tested in the anechoic chamber at the School of Mechanical Engineering at the University of Adelaide. The microphone holders were mounted in a plate with the microphone diaphragms sitting approximately 75 mm above the plate surface. High-density acoustic insulation was wedged around the microphones to prevent reflections from the plate arriving back at the microphone diaphragms. Initially, 60 mm thick Autex Quietstuf polyester insulation with a density of 30 kg/m^3 was used. After initial testing, the polyester insulation was replaced by 60 mm thick Dunlop Enduro Foam (EN 38-200) with a density of 38 kg/m^3. Figure 11 shows a photo of the microphone array and the foam wedged around the microphones.

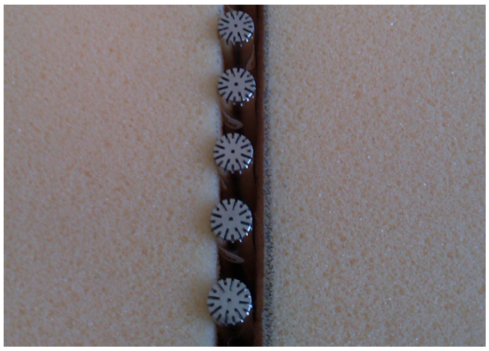

Figure 11 – Photo of array microphones with 60 mm thick Dunlop Enduro Foam (EN 38-200) wedged around microphones.

Beamforming measurements were conducted using a loudspeaker driven by a band-limited white noise signal with energy up to $1.25f_{\max}$. The axis of the loudspeaker was pointed to the centre of the microphone array to minimise the effect of loudspeaker directionality. The loudspeaker was moved to various source positions x_s while keeping the vertical distance to the array constant at $y_t = 28\lambda_{\min}$.

The data acquisition system consisted of an NI cDAQ-9178 chassis with 8 x NI 9234 modules that was configured using the MATLAB Data Acquisition Toolbox. For each measurement, 2 seconds of data at a sample rate of $3.2f_{\max}$ was recorded. Beampatterns were calculated based on the measured cross-spectral densities by focussing the array successively at target locations x_t extending from $-375\lambda_{\min}$ to $375\lambda_{\min}$.

Measured stationary source beampatterns

Figure 12(a) illustrates the beampattern measured with the loudspeaker positioned at $x_s = 47\lambda_{\min}$ and the polyester insulation wedged around the array microphones. In comparison to the theoretical free-field beampattern shown in Figure 13(b), which will be introduced below, the measured beampattern has wobbles in the main lobe and increased side lobe levels at frequencies of $0.67f_{\max}$ and $0.87f_{\max}$.

Figure 12(b) presents the theoretical beampattern for the case of including a reflection from the microphone holder plate. The reflection was modelled by including an additional image source at $[x_s, y_t + 2h]$ with $h = 75$mm the distance between the microphone diaphragms and microphone holder plate. The anomalies that appear in the resulting beampattern shown in Figure 12(b) are similar to the ones observed in the measured beampattern with the polyester insulation installed shown in Figure 12(a). This indicates that the anomalies are most likely caused by reflections from the microphone holder plate arriving back at the microphone with significant energy.

Figure 13(a) illustrates the beampattern measured after replacing the polyester insulation with a high density foam

product. The theoretical free-field beampattern is included in Figure 13(b) for comparison. The measured and theoretical beampatterns are very similar indicating that the problem caused by reflections has been resolved. Similar agreement between the measured and theoretical beampatterns was obtained for other loudspeaker positions.

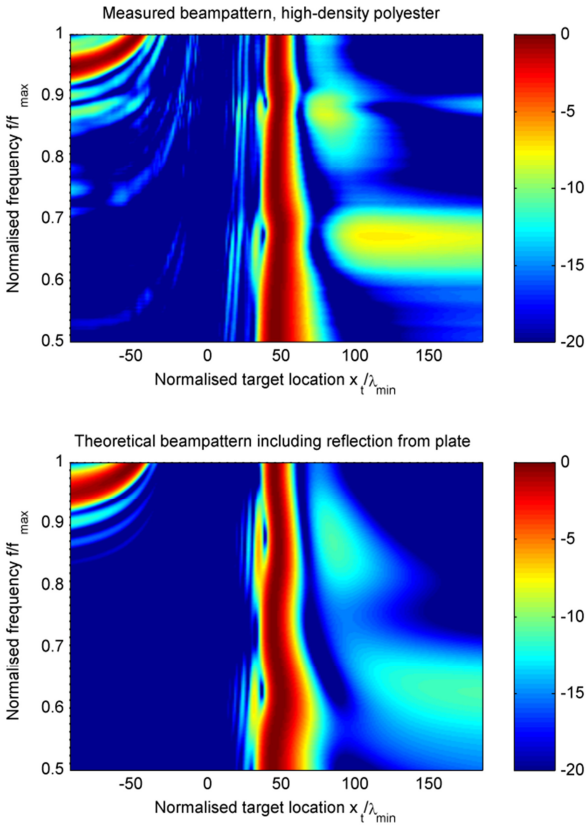

Figure 12 – (a) Measured beampattern with the loudspeaker positioned at $x_s = 47\lambda_{\min}$and $y_t = 28\lambda_{\min}$ and high density polyester insulation wedged around the array microphones. The array consists of $M = 30$ microphones spaced at $d = 0.58\lambda_{\min}$. (b) Theoretical beampattern including a reflection from the microphone holder plate.

CONCLUSION

Beamforming algorithms for moving acoustic sources include a de-Dopplerisation process that corrects for the Doppler shift in the received acoustic signals. This process successfully corrects for the Doppler shift associated with the measured source but not for interfering sources that are located away from the measured source. This leads to SNR enhancements that differ depending on whether the interfering source leads or lags the measured source as they move past the array. The de-Dopplerisation process also causes grating lobes associated with spatial aliasing to move to lower frequencies when the interfering source leads the measured source, and higher frequencies when it lags. The described effects can have a significant effect on the beamforming performance, especially for source-array arrangements and source speeds that result in rapidly changing Doppler shifts at the array microphones. When designing a microphone array for such scenarios, it is therefore important to conduct simulations that involve the use of a moving, rather than stationary, acoustic source.

ACKNOWLEDGEMENT

The work presented in the paper was funded by ARC Linkage Project LP110100529.

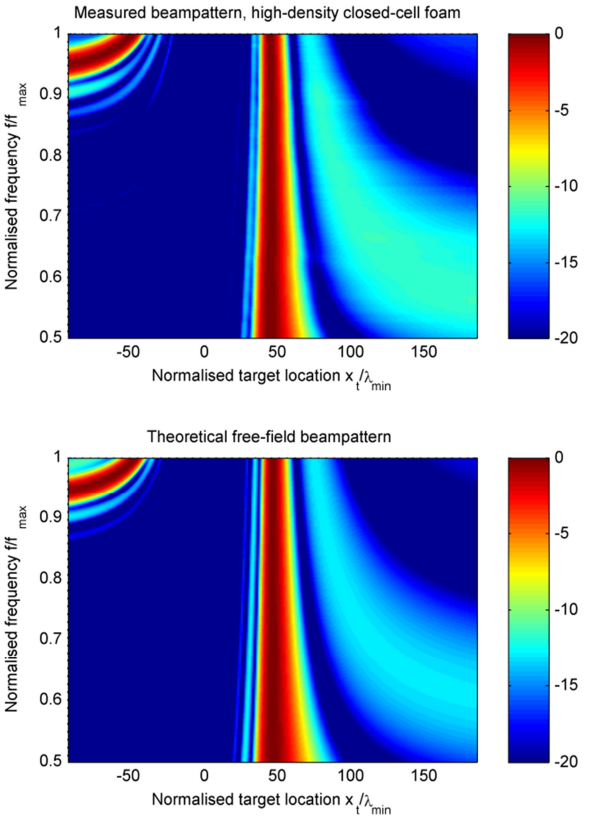

Figure 13 – Measured and theoretical free-field beampatterns with the loudspeaker positioned at $x_s = 47\lambda_{\min}$ and $y_t = 28\lambda_{\min}$ and high density foam wedged around the array microphones. The array consists of $M = 30$ microphones spaced at $d = 0.58\lambda_{\min}$.

REFERENCES

Brühl, S. and Röder, A. 2000, 'Acoustic noise source modelling based on microphone array measurements', *Journal of Sound and Vibration*, vol. 231, no. 3, pp. 611-617

Cohen, L. 1995, *Time-Frequency Analysis*, Prentice Hall, US

Fleury, V. and Bulté, J. 2011, 'Extension of deconvolution algorithms for the mapping of moving acoustic sources', *Journal of the Acoustical Society of America*, vol. 129, no. 3, pp. 1417-1428

Guérin, S., Weckmüller, C. and Michel, U. 2006, 'Beamforming and deconvolution for aerodynamic sound sources in motion', *Proceedings of the 1st Berlin Beamforming Conference*, November 21-22, Berlin, Germany, pp. 1-23.

Guérin, S. and Weckmüller, C. 2008, 'Frequency-domain reconstruction of the point-spread function for moving sources, *Proceedings of the 2nd Berlin Beamforming Conference*, 19-20 February, Berlin, Germany, pp. 1-23.

Guérin, S. and Siller, S. 2008, 'A hybrid time-frequency approach for the noise localization analysis of aircraft flyovers', *Proceedings of the 14th Aeroacoustics Conference*, 5-7 May, Vancouver, Canada, pp. 1-14.

Howell, G.P., Bradley, A.J., McCormick, M.A. and Brown, J.D. 1986, 'De-dopplerization and acoustic imaging of aircraft flyover noise measurements', *Journal of Sound and Vibration*, vol. 105, no. 1, pp. 151-167

Johnson, D.H. and Dudgeon, D.E. 1993, *Array Signal Processing: Concepts and Techniques*, Prentice Hall, USA

Siller, H.A. 2012, 'Localisation of sound sources on aircraft in flight', *Proceedings of the 4th Berlin Beamforming Conference*, Berlin, Germany, pp. 1-16.